AGU PUBLICATIONS

Geophysical Research Letters

RESEARCH LETTER
10.1002/2014GL060809

Key Points:
- Long waves attenuate with distance traveled in proportion to the inverse of wave period squared
- Significant wave height attenuates with distance traveled into the MIZ
- Peak periods increase with distance traveled into the MIZ

Correspondence to:
M. H. Meylan,
mike.meylan@newcastle.edu.au

Citation:
Meylan, M. ., L. G. Bennetts, and A. L. Kohout (2014), In situ measurements and analysis of ocean waves in the Antarctic marginal ice zone, *Geophys. Res. Lett.*, *41*, 5046–5051, doi:10.1002/2014GL060809.

Received 7 JUN 2014
Accepted 16 JUL 2014
Accepted article online 21 JUL 2014
Published online 30 JUL 2014

In situ measurements and analysis of ocean waves in the Antarctic marginal ice zone

Michael H. Meylan[1], Luke G. Bennetts[2], and Alison L. Kohout[3]

[1]School of Mathematical and Physical Science, University of Newcastle, Newcastle, New South Wales, Australia, [2]School of Mathematical Sciences, University of Adelaide, Adelaide, South Australia, Australia, [3]National Institute of Water and Atmospheric Research, Christchurch, New Zealand

Abstract In situ measurements of ocean surface wave spectra evolution in the Antarctic marginal ice zone are described. Analysis of the measurements shows significant wave heights and peak periods do not vary appreciably in approximately the first 80 km of the ice-covered ocean. Beyond this region, significant wave heights attenuate and peak periods increase. It is shown that attenuation rates are insensitive to amplitudes for long-period waves but increase with increasing amplitude above some critical amplitude for short-period waves. Attenuation rates of the spectral components of the wavefield are calculated. It is shown that attenuation rates decrease with increasing wave period. Further, for long-period waves the decrease is shown to be proportional to the inverse of the period squared. This relationship can be used to efficiently implement wave attenuation through the marginal ice zone in ocean-scale wave models.

1. Introduction

The response of Antarctic sea ice to climate change is poorly understood at present. It is characterized by pronounced regional variability. The inability of sea ice models to reproduce, for example, trends in observed Antarctic sea ice extent over the last 30 years reflects the lack of understanding of processes regulating Antarctic sea ice [*Turner et al.*, 2013].

Kohout et al. [2014] recently confirmed ocean surface waves have a detrimental impact on Antarctic ice cover. Southern Ocean waves penetrate hundreds of kilometers into the ice-covered ocean, before being fully attenuated by the ice cover. The waves define a dynamic region known as the marginal ice zone (MIZ). Floe sizes in the MIZ are relatively small due to wave-induced fracture. These small floes are mobile and susceptible to winds, currents, and melting in the summer. *Kohout et al.* [2014] used numerical models and satellite data to highlight a negative correlation between trends in local wave activity and trends in regional ice extent.

The findings of *Kohout et al.* [2014] imply ocean wave impacts on sea ice should be integrated into general circulation models used for climate studies. However, wave and sea ice model components are not coupled in contemporary general circulation models. Wave models generally do not operate in the ice-covered ocean, although the latest release of the WAVEWATCH III wave model permits this option [*Rogers and Zieger*, 2014]. Currently, sea ice models are not affected by wave processes directly.

Coupling between ocean wave and sea ice models will also help understand the retreat of Arctic sea ice in the era of climate change. *Francis et al.* [2011], *Khon et al.* [2014], and *Thomson and Rogers* [2014] used numerical models, in situ measurements and/or satellite data to show that the retreat is being accompanied by increasing wave activity. MIZ-like conditions can therefore be expected to proliferate in the Arctic and accelerate ice retreat [*Squire*, 2011].

Progress toward wave-ice model coupling is now being made. In particular, *Williams et al.* [2013a, 2013b] developed an idealized version of a coupled wave-ice model, which is now being integrated into an ice/ocean model version of the Hybrid Coordinate Ocean Model [*Williams et al.*, 2012]. Moreover, *Doble and Bidlot* [2013] extended the European Centre for Medium-Range Weather Forecasts's version of the WAM wave model into the ice-covered ocean.

Coupled wave-ice models rely on knowledge of the spectral evolution of waves in the ice-covered ocean, i.e., penetration distances of waves into the MIZ. Ocean waves are composed of a large number of spectral

components with different wave periods and, consequently, different wavelengths. A series of experiments conducted in the Arctic over 30 years ago showed spectral components of the wave spectrum attenuate at different rates [*Wadhams et al.*, 1988]. Long-period components tend to attenuate at slower rates than short-period components. Wave spectra therefore skew toward long periods, i.e., large wavelengths, with distance traveled into the MIZ, but a distinct relationship has yet to be found.

Mathematical models of wave attenuation in the ice-covered ocean, as a function of wave period, have subsequently been developed. The models can be roughly divided into two categories. First, models based on wave scattering theory—pioneered by Peter Wadhams, Vernon Squire and coworkers, and most recently *Bennetts and Squire* [2012a]. Second, models that treat the ice cover as a viscous [*Keller*, 1998] or viscoelastic [*Wang and Shen*, 2010] layer on the ocean surface. However, to date, model validation has been restricted by the lack of robust field data sets available [*Kohout and Meylan*, 2008; *Bennetts et al.*, 2010; *Bennetts and Squire*, 2012b].

The experiments reported and analyzed by *Wadhams et al.* [1988] were a milestone in terms of understanding how sea ice attenuates ocean waves. However, the methods used now appear outdated. For instance, wave measurements were made on single chart recorders, flown from floe to floe. Data analysis therefore required a strong assumption of a stationary wavefield.

Moreover, the prevailing ice conditions during the experiments are not representative of the Antarctic MIZ—nor many regions of the modern ice-covered Arctic Ocean. Measurements of waves in the Antarctic MIZ are scarce. Those measurements that do exist are taken from experiments not designed to measure wave attenuation. They are hence limited in terms of their spatial coverage. *Wadhams et al.* [2004] used synthetic aperture radar to measure waves in the pancake ice region of the Antarctic MIZ with the intent of using the data to determine ice thickness. *Hayes et al.* [2007] obtained measurements of wave activity in the Antarctic MIZ serendipitously from an autonomous underwater vehicle but only up to 10 km in from the ice edge. *Doble and Bidlot* [2013] compare measurements from a single wave buoy in pancake ice within the Weddell Sea with their model predictions, which includes a wave-induced ice breakup event.

An experimental campaign dedicated to measuring wave attenuation on a long transect of the Antarctic MIZ was conducted as part of the Australian Antarctic Division's second Sea Ice Physics and Ecosystem Experiment, 2012 [*Kohout and Williams*, 2013]. The experiments provided thousands of measurements of waves, simultaneously, at up to five locations, on a transect spanning up to 250 km.

Kohout et al. [2014] presented a preliminary data analysis of the measurements to support their finding that wave activity and ice extent are correlated. The analysis focused on large wave events and did not consider dependence of attenuation rates on wave periods.

A full spectral analysis of measured attenuation rates is conducted here. The spectral analysis is conducted to better understand the attenuation process. It is also necessary for use in spectral wave models, for example, WAM or WAVEWATCH III, and to help validate existing attenuation models and indicate directions for future model enhancements.

2. Waves in Ice Measurements

On 23 to 24 September 2012, five autonomous wave sensors were deployed on ice floes along a meridional transect of the Antarctic MIZ. The transect was located approximately 121.2°E and between 61.5°S and 62.5°S. The first sensor was deployed approximately 16 km from the ice edge and the last sensor approximately 130 km from the ice edge. The floes used were chosen to be large enough (greater than 10 m diameter) to provide confidence they could support the sensors for the 6 week battery life. The floes were also chosen small enough (less than 25 m diameter) to ensure their motions were consistent with the surrounding wavefield. Nevertheless, the motion of a floe of 25 m diameter is unlikely to be consistent with spectral components of the wavefield having wavelengths less than 100 m (using the rule of thumb that floes respond to waves with lengths less than 4 times their diameter). A 100 m wavelength corresponds to, approximately, an 8 s wave period, via the open (deep) water dispersion relation. However, the spectral analysis presented in section 3 considers wave periods as short as 6 s, as the results for small wave periods appear consistent with the larger wave periods. Note that wave periods of the spectral components of the wavefield are conserved in the ice-covered ocean, whereas wavelengths are expected to vary, especially for smaller periods.

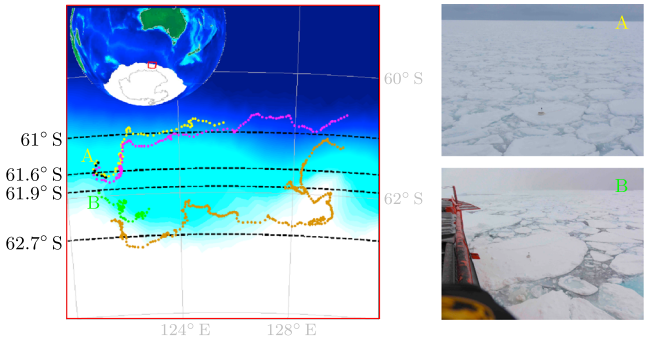

Figure 1. (left) Paths taken by wave sensors. Underlying color scheme is mean sea ice concentration. White represents ice concentrations greater than 45% and dark blue open water. Location of the experiment on global scale shown is shown in inset (top left-hand corner). White represents mean concentrations greater than 15%. (right) Two photos of ice conditions taken immediately after deployment of sensors.

Figure 1 shows the sensor tracks. The sensors drifted predominantly east and also trended north into open ocean. Drift caused the distance between the most northerly and most southerly sensors to extend up to 250 km. Generally, the sensors did not survive for the duration of their battery life. One sensor lasted for 1 day, two for 9 days, and one for 17 days. These sensors were victims of storms or, presumably, their host floe melting in open water. The sole exception was the sensor deployed deep into the MIZ, which lasted 39 days, before either its battery died or its host floe melted. This sensor survived for substantially longer than the others due to its distance from open water and the shielding effect of the MIZ from storm waves.

Each sensor comprised a high-resolution vertical accelerometer, a GPS, an iridium transceiver, and a processor. The sensors activated simultaneously for a 34 min period once every 3 h. Recorded acceleration time series were converted to wave spectra, $S(f)$ (m^2/Hz), where f denotes frequency in Hertz. These were relayed via satellite, along with sensor locations. The array of sensors therefore provided time series of wave spectra, as a function of penetration distance into the MIZ.

Calculation of the wave spectra involved dividing acceleration spectra by the response weights of frequency squared to map from accelerations to displacements, high- and low-pass filtering, and use of Welch's averaged periodogram method. The resulting power spectra were provided in 55 frequency bins, with corresponding wave periods ranging from approximately 5 s to 24 s. A. L. Kohout et al. (A device for measuring wave-induced motion of ice floes in the Antarctic marginal ice zone, submitted to *Annals of Glaciology*, 2014) give full details of the conversion algorithm. A five point moving average was used to smooth the measured wave spectra for the analysis conducted in section 3.

A camera installed on the upper deck of the ship monitored the floe size distribution during deployment of the sensors. Three sudden increases in the dominant floe size, with respect to distance traveled into the MIZ, divided the ice cover into bands. The dominant floe sizes and corresponding bands were determined from the camera images to be: 2 m to 3 m from 61°S to 61.6°S, 5 m to 6 m from 61.6°S to 61.9°S, 10 m to 20 m from 61.9°S to 62.7°S, and greater than 100 m south of 62.7°S. The corresponding mean sea ice concentrations in the bands from 23 to 24 September and over longitudes 120.5°E to 122°E are 21.0 %, 48.1 %, 49.8 %, and 57.6 %, respectively, where the final band is taken up to latitude 63°S (calculated using Nimbus-7 scanning multichannel microwave radiometer and Defense Meteorological Satellite Program (DMSP) Special Sensor Microwave/Imager Sounder (SSMIS) Passive Microwave Data) [*Cavalieri et al.*, 1996]. Figure 1 (right) shows example photos of the ice conditions in the first and third bands immediately following sensor deployment. The stationarity of the band structure and its variation with longitude are unknown.

3. Results and Analysis

Figure 2 is a box-and-whisker plot of the significant wave height, H_s, and peak period, T_p, as a function of latitude. These are average quantities commonly used to describe ocean wave spectra [*World Meteorological Organization*, 1998]. The boxes contain data between the 25th and 75th percentiles. The red lines are median values. The whiskers extend to the most extreme data points not more than 1.5 times the height of the box away from the box. The significant wave height is defined to be 4 times the standard deviation of the surface elevation, i.e.,

$$H_s = 4\sqrt{\int_0^\infty S(f)\,\mathrm{d}f}.$$

It is therefore related to the energy held in the wave spectrum. The peak period is the period of maximum energy in the wave spectrum.

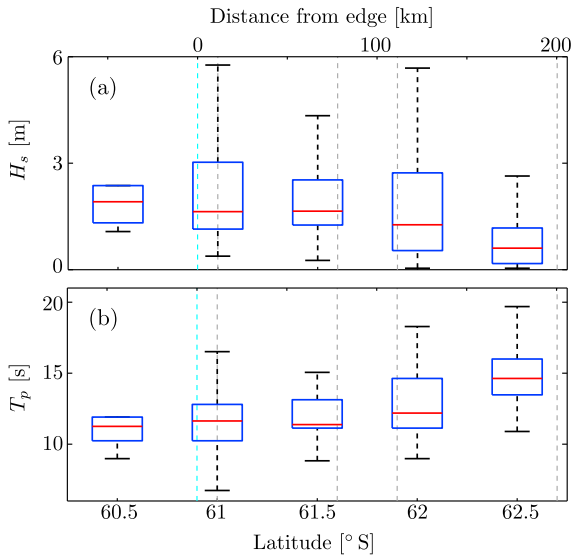

Figure 2. Box-and-whisker plots of (a) significant wave height, H_s, and (b) peak period, T_p, as functions of latitude. Mean ice edge (light blue broken lines) and floe size bands (grey) are overlaid on the plots.

Measured wave spectra are unreliable for the very small waves found deep into the MIZ. Therefore, only spectra with significant wave heights greater than 10^{-2} m are considered. Consequently, Figure 2 does not display significant wave heights and peak periods recorded in a vicinity of latitude 63°S.

Figure 2 shows that the significant wave height and peak period do not change appreciably in the first two floe-size bands of the MIZ, which is up to approximately 80 km in from the ice edge. In the subsequent bands the significant wave height attenuates and the peak period increases.

The attenuation rate of wave energy indicated by Figure 2a is required by numerical models to predict how far waves penetrate into the MIZ. It is most informative to examine the rate of attenuation of the different spectral elements individually. Therefore, consider the exponential attenuation rate of wave energy in the bin with corresponding spectral period $T = 1/f$, given by the attenuation coefficient $\alpha(T)$, which is defined as

$$\alpha(T) = \frac{\ln\{S_i(T)/S_j(T)\}}{D_{i,j}}. \quad (1)$$

Here S_i and S_j are wave spectra at adjacent sensors, where sensor i is at a higher latitude than sensor j, and $D_{i,j}$ is the corresponding distance between latitudes, i.e., waves are assumed to travel directly south. Only spectral values greater than 10^{-2} m^2/Hz are considered, as well as sensors with separations greater than 1 km.

Existing attenuation models usually assume linearity, i.e., the attenuation coefficient is independent of wave amplitude. To test this hypothesis here, a spectral amplitude, $A(T)$, corresponding to a bin with wave period T, is defined as [*Dean and Dalrymple*, 2000]

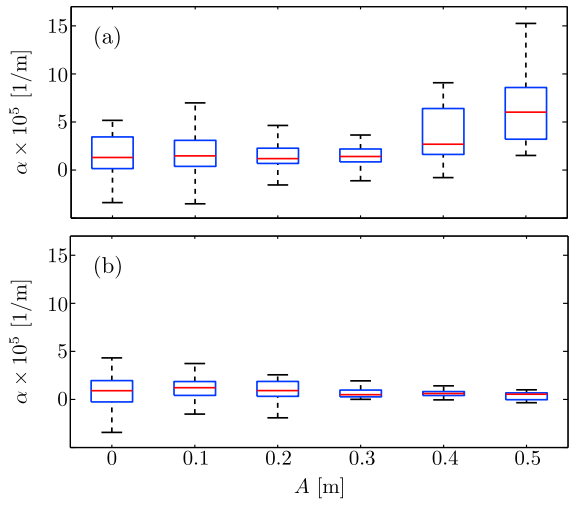

Figure 3. Box-and-whisker plots of the attenuation coefficient, α, as a function of spectral amplitude, A, for period bins (a) 11 s and (b) 15 s.

$$A(T) = \sqrt{2\int_{1/T-\frac{1}{2}\Delta f}^{1/T+\frac{1}{2}\Delta f} S(f)\,\mathrm{d}f}. \quad (2)$$

Figure 3 shows box-and-whisker plots of the attenuation coefficient as a function of spectral amplitude. The attenuation coefficient data are binned according to their closest spectral wave period. Results for two periods are presented, $T = 11$ s and $T = 15$ s, with $\Delta f = 0.002$. These periods are representative of short- and long- period regimes, respectively. The attenuation coefficient for a 15 s wave period is insensitive to wave amplitude. This indicates that the linear assumption is valid for the long-period regime.

The attenuation coefficient for a 11 s wave period is insensitive to spectral amplitudes, for amplitudes less than 0.3 m. However, for

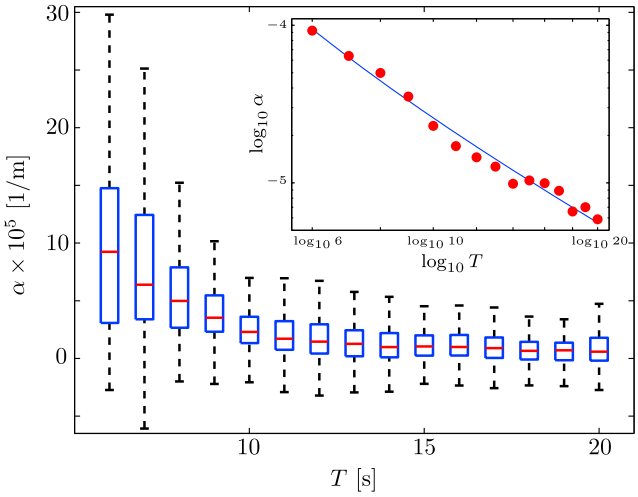

Figure 4. Box-and-whisker plot of the attenuation coefficient, α, as a function of period, T. Inset shows median values and a nonlinear least squares fit of the form given in equation (3).

amplitudes greater than 0.3 m, the attenuation coefficient increases with increasing amplitude. This indicates that, in the short-period regime, a transition occurs from linear theory holding to nonlinear processes affecting attenuation.

In general, the shorter the wave period, the smaller the amplitude at which the transition occurs. However, data are not sufficiently robust to conduct a thorough investigation of the onset of nonlinearities. Generally, the measured attenuation rates occupy the linear regime.

Figure 4 shows a box-and-whisker plot of the attenuation coefficient as a function of wave period. Data are binned irrespective of their associated spectral amplitudes. Data at the outlying wave periods of 5 s and 24 s are considered to be unreliable and are not shown. The 24 s period bin is too wide to provide information on spectral response. The 5 s bin is likely to be affected by local wave generation and wave interactions with the floes on which the sensors are deployed.

The results shown in Figure 4 display a clear trend for decreasing attenuation rate with increasing wave period. This is consistent with measurements of wave attenuation in the Arctic MIZ [e.g., *Wadhams et al.*, 1988]. The order of magnitude of the attenuation coefficient, 10^{-5} per meter, is also consistent with that reported in *Wadhams et al.* [1988].

The spread of attenuation coefficient values at a given period can be attributed to the following: nonstationarity of wave processes, variation in wave directions, nonlinearities, and changing ice conditions. However, the dependence of the attenuation coefficient on wave period is remarkably consistent. Note that previous measurements were not of sufficient resolution to allow a clear correlation between attenuation rates and wave period to be seen. The inset in Figure 4 emphasizes the consistency and indicates functional dependence of the attenuation coefficient on wave period. The inset shows a log-log plot of the median values of the attenuation coefficient and a nonlinear fit to the median values, of the form

$$\alpha(T) = \frac{a}{T^2} + \frac{b}{T^4}. \tag{3}$$

The coefficients $a = 2.12 \times 10^{-3}$ (s^2/m) and $b = 4.59 \times 10^{-2}$ (s^4/m) are calculated using a least squares regression.

The term a/T^2 dominates the nonlinear fit for wave periods greater than 10 s. The attenuation coefficient is therefore approximately proportional to $1/T^2$ in the long-period regime. For deep water waves in the open ocean, T^2 is proportional to the wavelength of the corresponding spectral component. Hence, assuming the presence of ice cover does not alter wavelengths of long-period waves appreciably, dependence on $1/T^2$ is equivalent to dependence on the reciprocal of the wavelength, i.e., the attenuation rate per wavelength is constant.

The term b/T^4 contributes to the nonlinear fit for wave periods less than 10 s. The attenuation coefficient therefore departs from being proportional to $1/T^2$, and hence the reciprocal of the open ocean wavelength, in the medium- to short-period regime.

4. Summary

An analysis of measurements of ocean surface waves in the Antarctic MIZ by an array of five wave sensors has been presented. The outer band of the MIZ, in which dominant floe sizes are less than 6 m and ice concentrations are relatively low, was shown to not affect the significant wave height or peak period of the

wavefield. Deeper into the MIZ, where dominant floe sizes are greater than 10 m and concentrations are higher, the significant wave height attenuates and the peak period increases.

Subsequent analysis focussed on exponential attenuation rates of the spectral components of the wavefield. The assumption of linearity of the attenuation process, which undergirds contemporary models, was tested. It was found that the linear assumption holds for long-period waves. However, evidence was found that nonlinear processes affect attenuation rates for short-period waves above some critical spectral amplitude.

To conclude, attenuation rates were shown to be order 10^{-5} per meter and to decrease with increasing wave period, which is consistent with previous findings. Further, median attenuation rates of wave period bins were shown to be approximated by a function of the form $a/T^2 + b/T^4$, where T denotes wave period and a and b are constants. Attenuation rates were therefore deduced to be proportional to the reciprocal of the wave period squared, in the long-period regime. This relationship could form the basis for parameterization of wave attenuation through the MIZ in ocean-scale wave models.

Acknowledgments

Inprod Pty Ltd designed and constructed the wave sensors. Martin Doble, Vernon Squire, and Tim Haskell contributed toward sensor design. The captain and crew of RSV *Aurora Australis* assisted in deploying the sensors. Takenobu Toyota provided floe size and ice thickness data. Alessandro Toffoli provided advice on wave analysis. The measurements were funded by the following: a New Zealand Foundation of Research Science and Technology Postdoctoral award to A.L.K.; the Marsden Fund Council, administered by the Royal Society of New Zealand; NIWA through core funding under the National Climate Centre Climate Systems program; the Antarctic Climate and Ecosystems Cooperative Research Centre; and the Australian Antarctic Science Grant Program (project 4073). M.H.M. acknowledges the support of the Office of Naval Research. L.G.B. acknowledges funding support from the Australian Research Council (DE130101571) and the Australian Antarctic Science Grant Program (project 4123). The data used for this study are available through the Australian Antarctic Data Centre [*Kohout and Williams*, 2013].

The Editor thanks two anonymous reviewers for their assistance in evaluating this paper.

References

Bennetts, L. G., and V. A. Squire (2012a), On the calculation of an attenuation coefficient for transects of ice-covered ocean, *Proc. R. Soc. London, Ser. A*, *468*(2137), 136–162.

Bennetts, L. G., and V. A. Squire (2012b), Model sensitivity analysis of scattering-induced attenuation of ice-coupled waves, *Ocean Model.*, *45–46*, 1–13.

Bennetts, L. G., M. A. Peter, V. A. Squire, and M. H. Meylan (2010), A three-dimensional model of wave attenuation in the marginal ice zone, *J. Geophys. Res.*, *115*, C12043, doi:10.1029/2009JC005982.

Cavalieri, D. J., C. L. Parkinson, P. Gloersen, and H. Zwally (1996), Sea ice concentrations from Nimbus-7 SMMR and DMSP SSM/I-SSMIS passive microwave data, *Tech. Rep. USA: NASA 278DAAC*, National Snow and Ice Data Center, Boulder, Colo.

Dean, R. G., and R. A. Dalrymple (2000), *Water Wave Mechanics for Engineers and Scientists*, vol. 2, *Advanced Series on Ocean Engineering*, 353 pp., World Scientific, Singapore.

Doble, M. J., and J. R. Bidlot (2013), Wave buoy measurements at the Antarctic sea ice edge compared with an enhanced ECMWF WAM: Progress towards global waves-in-ice modelling, *Ocean Model.*, *70*, 166–173.

Francis, O. P., G. G. Panteleev, and D. E. Atkinson (2011), Ocean wave conditions in the Chukchi sea from satellite and in situ observations, *Geophys. Res. Lett.*, *38*, L24610, doi:10.1029/2011GL049839.

Hayes, D. R., A. Jenkins, and S. McPhail (2007), Autonomous underwater vehicle measurements of surface wave decay and directional spectra in the marginal sea ice zone, *J. Phys. Oceanogr.*, *37*(1), 71–83.

Keller, J. B. (1998), Gravity waves on ice-covered water, *J. Geophys. Res.*, *103*(C4), 7663–7669, doi:10.1029/97JC02966.

Khon, V. C., I. I. Mokhov, F. A. Pogarskiy, A. Babanin, K. Dethloff, A. Rinke, and H. Matthes (2014), Wave heights in the 21st century Arctic Ocean simulated with a regional climate model, *Geophys. Res. Lett.*, *41*, 2956–2961, doi:10.1002/2014GL059847.

Kohout, A. L., and M. H. Meylan (2008), An elastic plate model for wave attenuation and ice floe breaking in the marginal ice zone, *J. Geophys. Res.*, *113*, C09016, doi:10.1029/2007JC004434.

Kohout, A. L., and M. J. M. Williams (2013), Waves-in-ice observations made during the SIPEX II voyage of the Aurora Australis, 2012, *Tech. Rep.*, Australian Antarctic Data Centre, Hobart, Tasmania, Australia, doi:10.4225/15/53266BEC9607F.

Kohout, A. L., M. J. M. Williams, S. Dean, and M. H. Meylan (2014), Storm-induced sea ice breakup and the implications for ice extent, *Nature*, *509*, 604–607, doi:10.1038/Nature13262.

Rogers, W. E., and S. Zieger (2014), User manual and system documentation of WAVEWATCH III(R) version 4.18b, chap. S_{ice}: Damping by sea ice, edited by H. Tolman, pp. 60–61, *Tech. Note, MMAB Contribution 316*, NOAA/NWS, College Park, Md.

Squire, V. A. (2011), Past, present and impendent hydroelastic challenges in the polar and sub polar seas, *Philos. Trans. R. Soc. London, Ser. A*, *369*, 2813–2831.

Turner, J., T. J. Bracegirdle, T. Phillips, G. J. Marshall, and J. S. Hosking (2013), An initial assessment of Antarctic sea ice extent in the CMIP5 models, *J. Clim.*, *26*, 1473–1484.

Thomson, J., and W. E. Rogers (2014), Swell and sea in the emerging Arctic Ocean, *Geophys. Res. Lett.*, *41*, 3136–3140, doi:10.1002/2014GL059983.

Wadhams, P., V. A. Squire, D. J. Goodman, A. M. Cowan, and S. C. Moore (1988), The attenuation rates of ocean waves in the marginal ice zone, *J. Geophys. Res.*, *93*(C6), 6799–6818.

Wadhams, P., F. F. Parmiggiani, G. de Carolis, D. Desiderio, and M. J. Doble (2004), SAR imaging of wave dispersion in Antarctic pancake ice and its use in measuring ice thickness, *Geophys. Res. Lett.*, *31*(15), L15305, doi:10.1029/2004GL020340.

Wang, R., and H. Shen (2010), Gravity waves propagating into an ice-covered ocean: A viscoelastic model, *J. Geophys. Res.*, *115*, C06024, doi:10.1029/2009JC005591.

Williams, T. D., L. G. Bennetts, V. A. Squire, and D. Dumont (2012), Preliminary results from a two-dimensional model of wave-ice interactions in the Fram Strait, in *Proceedings of the Arctic Technology Conference, 2012*, vol. 2, pp. 1071–1078, Society of Petroleum Engineers, Houston, Tex.

Williams, T. D., L. G. Bennetts, D. Dumont, V. A. Squire, and L. Bertino (2013a), Wave-ice interactions in the marginal ice zone. Part 1: Theoretical foundations, *Ocean Model.*, *71*, 81–91.

Williams, T. D., L. G. Bennetts, D. Dumont, V. A. Squire, and L. Bertino (2013b), Wave-ice interactions in the marginal ice zone. Part 2: Numerical implementation and sensitivity studies along 1D transects of the ocean surface, *Ocean Model.*, *71*, 92–101.

World Meteorological Organization (1998), *Guide to Wave Forecasting and Analysis,* 2nd ed., p. 702, WMO, Geneva, Switzerland.